

Supervised Learning for Non-Sequential Data with the Canonical Polyadic Decomposition

Alexandros Haliassos*, Kriton Konstantinidis*, and Danilo P. Mandic, *Fellow, IEEE*

Abstract—There has been growing interest, both theoretical and practical, in utilizing tensor networks (TNs) for the analysis and design of machine learning systems. TNs have been shown to be able to handle both dense data (e.g., standard regression or classification tasks) and sparse data (e.g., recommender systems and one-hot encoded categorical features), unlike support vector machines and traditional deep learning techniques. Such a tensor-based framework can be interpreted as an application of local feature mappings to the data, which, through the outer product operator, allows for modelling all interactions of functions of the features; the corresponding weights are represented as a tensor network for computational tractability. In this paper, we derive efficient prediction and learning algorithms for supervised learning using the Canonical Polyadic (CP) decomposition, including suitable regularization and initialization schemes. We empirically demonstrate that the CP-based model performs at least on par with the existing models based on the Tensor Train (TT) decomposition on standard non-sequential tasks, while it outperforms TT-based models on MovieLens 100K dataset. Furthermore, in contrast to previous works which apply two-dimensional local feature maps to the data, we generalize the framework to handle arbitrarily high-dimensional maps, which equips the tensor-based models with enhanced expressiveness. We also propose a normalized version of the feature maps to address the stability and generalization capabilities. Our experiments show that this leads to dramatic improvements over the existing unnormalized and/or two-dimensional maps, as well as to a level of performance on non-sequential supervised learning tasks which is comparable with other machine learning models, including fully-connected neural networks.

Index Terms—Tensor Networks, Canonical Polyadic Decomposition, Supervised Learning, Non-Sequential Data, Regression, Classification, Recommender Systems

I. INTRODUCTION

Tensor networks (TNs) have recently found application in supervised learning, owing to their interpretable, modular structure and their ability to circumvent the curse of dimensionality by representing high-order tensors, i.e., multi-way arrays, by a set of interconnected lower-order tensors. For example, by establishing links between common TNs such as the Tensor Train (TT) [1] or Hierarchical Tucker (HT) networks [2], and deep learning architectures such as Recurrent [3], [4] or Convolutional Neural Networks [5], it has been possible to obtain both new theoretical insights [6], [7], [8] and practical advantages, especially in terms of dimensionality reduction. Indeed, TNs have proven to be useful for heavy compression of feedforward, convolutional, and recurrent networks, without a significant loss in performance [9], [10], [11].

The authors with an asterisk (*) contributed equally to this work.

All authors are with the Department of Electrical and Electronic Engineering, Imperial College London, London SW7 2AZ, U.K. (e-mails: {alexandros.haliassos14, k.konstantinidis19, d.mandic}@imperial.ac.uk)

This paper focuses on a related line of research, whereby TNs are employed for the design of scalable, interpretable, and general supervised learning models for multidimensional data. More specifically, we consider a recently introduced TN learning framework [12], [13] that can be interpreted as an application of local feature maps, followed by the outer product operator, to construct a rank-1 tensor which contains all possible interactions between features. The prediction is then performed through an inner product of the so-constructed rank-1 tensor with the corresponding weight tensor, whereby for affordable computations, the exponentially-scaled (with the respect to the number of features) original weight tensor is represented by a compact TN. By virtue of the TT and matrix TT formats of TNs, it has been made possible to obtain competitive results on tasks such as image recognition, recommender systems, and sequence-to-sequence learning [12], [13], [14].

Overall, the advantages of tensor network models include:

- linear scaling with the dimensionality of the feature vectors and constant scaling with the training size (assuming mini-batch gradient descent in training), making them suitable for big data applications;
- enhanced interpretability, due to the multi-linear nature of the model, that is not possible to achieve with other state-of-the-art. approaches such as neural networks and Support Vector Machines (SVMs);
- their inherent universal function approximation property for large enough dimension of the local feature maps;
- suitability for a wide range of supervised learning settings, including recommender systems, for which standard models such as neural networks and SVMs tend to underperform;
- potential to derive novel computationally tractable machine learning models using multilinear algebra together with gaining theoretical insights into the existing approaches.

Previous work on this paradigm has (either explicitly or implicitly) locally mapped the features to two-dimensional vectors, i.e., the *local dimension* of the mapping was two. However, we argue that the ability to increase the local dimension plays a critical role in the expressiveness of the models (they can only enjoy the universal function approximation property if the local dimension is large enough). On the other hand, this leads to significant computational costs for learning algorithms that do not scale linearly with the local dimension, such as in the work of [12], together with instability or poor generalization, depending on the feature map used.

In this work, we focus on the well-established Canonical Polyadic (CP) decomposition algorithm to represent the weight tensor of the model considered and refer to this model as the *CP-based model* (similarly, we refer to the models based on TT as *TT-based*). Compared with TT-based models, the use of CP has the following advantages:

- It allows for simpler optimization algorithms.
- The CP-based models can lead to more parsimonious and interpretable representations.
- Robustness to feature permutations, a desirable property for non-sequential data.

We derive prediction and learning algorithms, as well as the corresponding initialization and regularization schemes, that scale linearly with the dimensionality of the features and the local dimension, a key property for practical applications. The proposed model is also shown to exhibit performance which is similar or better compared with the TT-based counterparts on a class of non-sequential learning tasks considered, including the MovieLens 100K recommender system dataset.

A further contribution (that is agnostic to the type of decomposition used) is the generalization from the currently used two-dimensional feature maps to arbitrary d -dimensional maps; in this way, the framework is equipped with the ability to model all interactions of features raised to powers of up to $(d - 1)$. To avoid erratic behavior of the learning procedure for a high local dimension d , we propose to unit-normalize the feature vectors after mapping. Through experiments, it is demonstrated that a higher d can dramatically enhance performance and that the algorithms remain stable even for $d > 100$. The performance enhancement achieved through an increase in d is shown to enable the proposed models to exhibit competitive results over other popular models, including SVMs and feedforward neural networks.

The CP-based model has been implemented as a custom layer in TensorFlow 2.0 to enable straightforward experimentation with various optimizers, regularizers, and loss functions.¹

The rest of the paper is organized as follows. We first present the tensor preliminaries necessary to follow this work (Section II). Next, the tensor network framework for supervised learning is described, which forms a basis of our algorithm (Section III). After a discussion on the interpretability of the model and its universal function approximation property (Section IV), we present the derivations and algorithms for model prediction and learning (Section V). Local feature maps for different settings (Section VI) are subsequently considered and procedures for order regularization [13] are derived (Section VII). Next, model initialization is addressed (Section VIII), followed by a discussion on links between the CP-based model and related works as well as the advantages of our approach (Section IX). Finally, we provide experimental results (Section X), and we conclude with future research directions (Section XI).

II. PRELIMINARIES

The notation and definitions necessary to follow this work are given below; for a more comprehensive review of TDs and TNs, see [15], [16], [17].

A. Tensor Notation and Basic Operations

A real-valued tensor is a multidimensional array, denoted by a calligraphic font, e.g., $\mathcal{X} \in \mathbb{R}^{I_1 \times \dots \times I_N}$, where N is the order of the tensor, and I_n ($1 \leq n \leq N$) the size of its n^{th} mode. Matrices (denoted by bold capital letters, e.g., $\mathbf{X} \in \mathbb{R}^{I_1 \times I_2}$) can be seen as second order tensors ($N = 2$), vectors are denoted by bold lower-case letters, e.g., $\mathbf{x} \in \mathbb{R}^I$ and can be seen as order-1 tensors ($N = 1$), and scalars (denoted by lower-case letters, e.g., $x \in \mathbb{R}$) are tensors of order $N = 0$. A specific entry of a tensor $\mathcal{X} \in \mathbb{R}^{I_1 \times \dots \times I_N}$ is given by $x_{i_1, \dots, i_N} \in \mathbb{R}$. Moreover, we adopt a graphical notation, whereby a tensor is represented by a shape (e.g., a circle) with outgoing edges; the number of edges equals the order of the tensor (see [17] for more information on this graphical notation).

The following conventions for basic linear/multilinear operations are employed throughout the paper.

Definition 1 (Multi-Index). A *multi-index (in reverse lexicographic ordering)* is defined as $\bar{i}_1 \bar{i}_2 \dots \bar{i}_N = i_1 + (i_2 - 1)I_1 + (i_3 - 1)I_1 I_2 + \dots + (i_N - 1)I_1 \dots I_{N-1}$.

Definition 2 (Tensor Matricization). The *mode- n matricization* of a tensor $\mathcal{X} \in \mathbb{R}^{I_1 \times \dots \times I_N}$ reshapes the multidimensional array into a matrix $\mathbf{X}_{(n)} \in \mathbb{R}^{I_n \times I_1 I_2 \dots I_{n-1} I_{n+1} \dots I_N}$ with $(x_{(n)})_{i_n, \bar{i}_1 \dots \bar{i}_{n-1} \bar{i}_{n+1} \dots \bar{i}_N} = x_{i_1, \dots, i_N}$.

Definition 3 (Outer Product). The *outer product* of two vectors $\mathbf{a} \in \mathbb{R}^I$ and $\mathbf{b} \in \mathbb{R}^J$ is given by $\mathbf{c} = \mathbf{a} \circ \mathbf{b} \in \mathbb{R}^{I \times J}$ with $c_{i,j} = a_i b_j$.

Definition 4 (Kronecker Product). The *Kronecker product* of two matrices $\mathbf{A} \in \mathbb{R}^{I \times J}$ and $\mathbf{B} \in \mathbb{R}^{K \times L}$ is denoted by $\mathbf{C} = \mathbf{A} \otimes \mathbf{B} \in \mathbb{R}^{I \times J \times K \times L}$ with $c_{(i-1)K+k, (j-1)L+l} = a_{i,j} b_{k,l}$.

Definition 5 (Khatri-Rao Product). The *Khatri-Rao product* of two matrices $\mathbf{A} = [\mathbf{a}_1, \dots, \mathbf{a}_R] \in \mathbb{R}^{I \times R}$ and $\mathbf{B} = [\mathbf{b}_1, \dots, \mathbf{b}_R] \in \mathbb{R}^{J \times R}$ is denoted by $\mathbf{C} = \mathbf{A} \odot \mathbf{B} \in \mathbb{R}^{I \times J \times R}$, where the columns $\mathbf{c}_r = \mathbf{a}_r \otimes \mathbf{b}_r$, $1 \leq r \leq R$.

Definition 6 (Hadamard Product). The *Hadamard product* of two N^{th} -order tensors, $\mathcal{A} \in \mathbb{R}^{I_1 \times \dots \times I_N}$ and $\mathcal{B} \in \mathbb{R}^{I_1 \times \dots \times I_N}$ is denoted by $\mathcal{C} = \mathcal{A} \otimes \mathcal{B} \in \mathbb{R}^{I_1 \times \dots \times I_N}$ with $c_{i_1, \dots, i_N} = a_{i_1, \dots, i_N} b_{i_1, \dots, i_N}$.

Definition 7 (Tensor Contraction). The *contraction* of an N^{th} -order tensor, $\mathcal{A} \in \mathbb{R}^{I_1 \times \dots \times I_N}$ and an M^{th} -order tensor $\mathcal{B} \in \mathbb{R}^{J_1 \times \dots \times J_M}$ over the n^{th} and m^{th} modes respectively, where $I_n = J_m$, results in an $(N + M - 2)^{\text{th}}$ -order tensor with entries $c_{i_1, \dots, i_{n-1}, i_{n+1}, \dots, i_N, j_1, \dots, j_{m-1}, j_{m+1}, \dots, j_M} = \sum_{i_n=1}^{I_n} a_{i_1, \dots, i_{n-1}, i_n, i_{n+1}, \dots, i_N} b_{j_1, \dots, j_{m-1}, i_n, j_{m+1}, \dots, j_M}$.

Definition 8 (Inner Product of Tensors). The *inner product* of two N^{th} -order tensors $\mathcal{A} \in \mathbb{R}^{I_1 \times \dots \times I_N}$ and $\mathcal{B} \in \mathbb{R}^{I_1 \times \dots \times I_N}$ is denoted by $c = \langle \mathcal{A}, \mathcal{B} \rangle \in \mathbb{R}$ with $c = \sum_{i_1, \dots, i_N} a_{i_1, \dots, i_N} b_{i_1, \dots, i_N}$.

¹https://github.com/KritonKonstantinidis/CPD_Supervised_Learning

A property (see Appendix A for proof) used in this paper is

$$\begin{aligned} & \left(\mathbf{A}^{(1)} \odot \dots \odot \mathbf{A}^{(N)} \right)^T \left(\mathbf{B}^{(1)} \odot \dots \odot \mathbf{B}^{(N)} \right) \\ &= \mathbf{A}^{(1)T} \mathbf{B}^{(1)} \otimes \dots \otimes \mathbf{A}^{(N)T} \mathbf{B}^{(N)} \\ &= \left(\bigstar_{k=1}^N \mathbf{A}^{(k)T} \mathbf{B}^{(k)} \right), \end{aligned} \quad (1)$$

where $\mathbf{A}^{(k)} \in \mathbb{R}^{I_k \times J}$ and $\mathbf{B}^{(k)} \in \mathbb{R}^{I_k \times L}$.

B. Tensor Train and Canonical Polyadic Decompositions

Tensor Networks: A tensor network (TN) provides an efficient representation of a tensor through a set of lower-order tensors which are contracted over certain modes. The relatively low order of the core tensors within TNs and their sparse interconnections allow for the mitigation of the curse of dimensionality as the number of parameters within the TN representation tends to scale linearly with the tensor order (rather than exponentially as in the raw tensor format).

Tensor Train Decomposition: A tensor $\mathcal{X} \in \mathbb{R}^{I_1 \times \dots \times I_N}$ can be represented in the Tensor Train (TT) format as

$$\mathcal{X} = \mathcal{G}^{(1)} \times^1 \dots \times^1 \mathcal{G}^{(N)}, \quad (2)$$

where $\mathcal{G}^{(n)} \in \mathbb{R}^{R_{n-1} \times I_n \times R_n}$, $R_0 = R_N = 1$, are the TT cores, and $\mathcal{G}^{(n)} \times^1 \mathcal{G}^{(n+1)}$ denotes contraction over the last mode of $\mathcal{G}^{(n)}$ and first mode of $\mathcal{G}^{(n+1)}$. The TT rank is given by the dimensions of the contracted modes, i.e., TT rank = $\{R_1, \dots, R_{N-1}\}$. The TT format is depicted in the left panel of Fig. 1.

Canonical Polyadic Decomposition: The Canonical Polyadic (CP) decomposition [18], [19] expresses a tensor $\mathcal{X} \in \mathbb{R}^{I_1 \times \dots \times I_N}$ as a sum of outer products of vectors $\mathbf{a}_r^{(1)}, \mathbf{a}_r^{(2)}, \dots, \mathbf{a}_r^{(N)}$ (i.e., rank-1 terms):

$$\mathcal{X} = \sum_{r=1}^R \mathbf{a}_r^{(1)} \circ \dots \circ \mathbf{a}_r^{(N)} = \sum_{r=1}^R \bigcirc_{k=1}^N \mathbf{a}_r^{(k)}, \quad (3)$$

where R is the CP rank of the tensor (equal to the standard matrix rank when $N = 2$). We can arrange these vectors into N factor matrices $\mathbf{A}^{(n)} = [\mathbf{a}_1^{(n)}, \dots, \mathbf{a}_R^{(n)}] \in \mathbb{R}^{I_n \times R}$, ($1 \leq n \leq N$), which allows the CP decomposition to be expressed as a contraction of the identity tensor, $\mathcal{I} \in \mathbb{R}^{I_1 \times \dots \times I_N}$ (all ones on the super-diagonal) with the so-formed factor matrices. This view allows the CP decomposition to be formulated as a TN, as is shown in the right panel in Fig. 1.

Notice that the entries of the CP decomposition can be expressed as

$$\begin{aligned} x_{i_1, \dots, i_N} &= \sum_{r=1}^R a_{i_1, r}^{(1)} a_{i_2, r}^{(2)} \dots a_{i_N, r}^{(N)} \\ &= \left(\bigstar_{k=1}^N \hat{\mathbf{a}}_{i_k}^{(k)} \right) \mathbf{1}, \end{aligned} \quad (4)$$

where $\hat{\mathbf{a}}_j^{(n)}$ denotes the j^{th} row of the n^{th} factor matrix, and $\mathbf{1} = [1, \dots, 1]^T \in \mathbb{R}^R$.

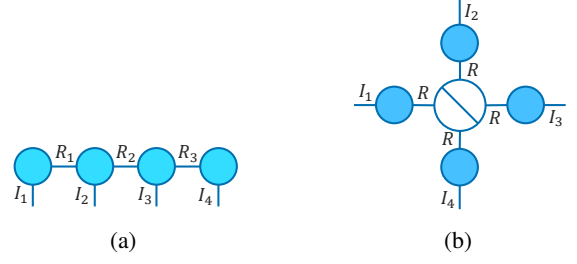


Fig. 1: Tensor network notation of an order-4 tensor. (a) Tensor Train and (b) Canonical Polyadic decomposition. A circle with a diagonal line denotes a super-diagonal tensor, in this case the identity tensor, with all unities on the diagonal.

Upon the matricization of the tensor \mathcal{X} , we obtain

$$\begin{aligned} \mathbf{X}_{(n)} &= \mathbf{A}^{(n)} \left(\mathbf{A}^{(N)} \odot \dots \odot \mathbf{A}^{(n+1)} \odot \mathbf{A}^{(n-1)} \right. \\ &\quad \left. \odot \dots \odot \mathbf{A}^{(1)} \right)^T \\ &= \mathbf{A}^{(n)} \left(\bigcirc_{\substack{k=N \\ k \neq n}}^1 \mathbf{A}^{(k)} \right)^T. \end{aligned} \quad (5)$$

Furthermore, the vectorization of \mathcal{X} can be expressed as

$$\text{vec}(\mathcal{X}) = \left(\bigcirc_{k=N}^1 \mathbf{A}^{(k)} \right) \mathbf{1}. \quad (6)$$

III. TENSOR NETWORK FRAMEWORK FOR SUPERVISED LEARNING

Consider a supervised learning task where each sample is represented as a set of N features. Now, consider a local feature mapping $\phi: \mathbb{R} \rightarrow \mathbb{R}^d$, which is applied to every feature x_n , where d is referred to as the *local dimension* of the mapping. The choice of the feature map is flexible and application-dependent. Upon taking the outer product between the mapped feature vectors, we obtain

$$\Phi(\mathbf{x}) = \bigcirc_{k=1}^N \phi(x_k) \in \mathbb{R}^{d^N}, \quad (7)$$

where \mathbb{R}^{d^N} is shorthand for $\mathbb{R}^{\overbrace{d \times \dots \times d}^{N \text{ times}}}$. The prediction produced by the model in (7) for one output (e.g., single-target regression or binary classification) is then given by

$$f(\mathbf{x}) = \langle \Phi(\mathbf{x}), \mathcal{W} \rangle, \quad (8)$$

where $\mathcal{W} \in \mathbb{R}^{d^N}$ is the *weight tensor*, which comprises all model coefficients. Note that in the case of multi-target regression or multi-class classification with L labels, the model is composed of L different weight tensors \mathcal{W}^l ($1 \leq l \leq L$). For simplicity, we consider only the single-target case in this paper, but the analysis can easily be generalized. For a graphical representation of the prediction of the model in (8) in tensor network notation, see Figure 2.

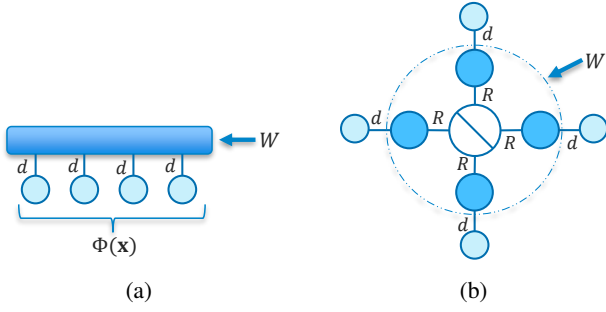


Fig. 2: Tensor-valued model prediction. (a) Without a tensor decomposition, (b) with CP decomposition of the weight tensor \mathcal{W} .

Example 1. Consider the map ϕ such that $\phi(x_n) = [1, x_n]^T$. Then, for the number of features $N = 3$, we have $\Phi(\mathbf{x}) \in \mathbb{R}^{2 \times 2 \times 2}$ and

$$f(\mathbf{x}) = w_{1,1,1} + w_{2,1,1}x_1 + w_{1,2,1}x_2 + w_{1,1,2}x_3 + w_{2,2,1}x_1x_2 \\ + w_{2,1,2}x_1x_3 + w_{1,2,2}x_2x_3 + w_{2,2,2}x_1x_2x_3. \quad (9)$$

Thus, the model in this case captures all combinations of distinct features, x_1, x_2, x_3 .

Observe from (9) that the size of the weight tensor, \mathcal{W} , scales exponentially with the number of features and is therefore computationally prohibitive to learn. To this end, it is possible to represent \mathcal{W} as a tensor network [12], where the number of parameters scales linearly in the feature dimension.

In this work, we represent \mathcal{W} in the CP format, which, unlike the TT format, is insensitive to the ordering of the features (see IX-A). Although this also holds true for the Tucker decomposition [15], using the Tucker format comes at a cost of exponential scaling with the number of features. Also, the Tucker decomposition involves a core tensor, the modes of which typically have dimensions smaller than those of the original tensor, thus rendering the Tucker decomposition unsuitable for weight tensors with dimensions 2 across all modes, such as in Example 1.

IV. CP-BASED MODEL

A. Model Prediction and Interpretability

It is important to notice that the model prediction can be expressed in terms of the rows of the factor matrices of the CP decomposition and the corresponding elements of the feature mapping in the form

$$f(\mathbf{x}) = \sum_{i_1, \dots, i_N} w_{i_1, \dots, i_N} \prod_{k=1}^N \phi(x_k)_{i_k} \quad (10)$$

$$= \sum_{i_1, \dots, i_N} \left(\bigotimes_{k=1}^N \hat{\mathbf{a}}_{i_k}^{(k)} \right) \mathbf{1} \prod_{k=1}^N \phi(x_k)_{i_k}. \quad (11)$$

In other words, the coefficient for each (transformed) feature interaction can be readily obtained after training simply by performing a Hadamard product of the corresponding row vectors of the learned factor matrices and then by summing over all entries of the resulting vector. This provides enhanced interpretability over SVMs or deep learning techniques, as the

importance of a given feature interaction can be observed in $\mathcal{O}(NRd)$ time.

Example 2. Consider again $\phi(x_n) = [1, x_n]^T$ with $N = 3$. Then, the coefficient for e.g., x_1x_3 could be obtained by finding the Hadamard product of $\hat{\mathbf{a}}_2^{(1)}$, $\hat{\mathbf{a}}_1^{(2)}$, and $\hat{\mathbf{a}}_2^{(3)}$, and then summing over the entries.

B. Universal Approximation Property

Recall that the TN framework discussed in Section III can approximate any function with an arbitrary approximation error, as long as the local feature dimension d is large enough [6]. Since there always exists a CP rank for which a tensor can be exactly decomposed in its CP form, the proposed model also satisfies the universal function approximation property. This highlights the importance of using a higher local dimension d for the feature map, rather than constraining it to 2.

Example 3. Consider $\phi(x_n) = [1, x_n, x_n^2, \dots, x_n^{(d-1)}]^T$; then, by allowing d and R to be sufficiently large, the model in (11) can capture any polynomial function. By Stone-Weierstrass theorem [20], there exist d and R such that the proposed model can approximate arbitrarily well any continuous function on compact subsets of \mathbb{R}^N .

V. EFFICIENT ALGORITHMS FOR PREDICTION

This section addresses efficient algorithms for prediction, based on the proposed model, as well as for learning the model parameters. For rigor, the mathematical derivations of the proposed algorithms are included; we refer the reader to the graphical notation to gain intuition on the underlying algorithms.

A. Prediction Algorithm

Given the factor matrices $\mathbf{A}^{(n)}$ and the map ϕ , there are various ways of obtaining model predictions, some of which are dramatically more computationally efficient than others. For example, a direct implementation of (8) would yield a procedure that scales exponentially with N .

To arrive at an efficient procedure for computing the model prediction, we express it as

$$f(\mathbf{x}) = \langle \Phi(\mathbf{x}), \mathcal{W} \rangle \\ = \langle \text{vec}(\Phi(\mathbf{x})), \text{vec}(\mathcal{W}) \rangle \\ = \text{vec}(\Phi(\mathbf{x}))^T \text{vec}(\mathcal{W}) \\ = \left(\bigotimes_{k=1}^N \phi(x_k) \right)^T \left(\bigotimes_{k=1}^N \mathbf{A}^{(k)} \right) \mathbf{1} \\ = \left(\bigotimes_{k=1}^N \phi^T(x_k) \mathbf{A}^{(k)} \right) \mathbf{1}. \quad (12)$$

The corresponding computation procedure is given in Algorithm 1, the complexity² of which is $\mathcal{O}(NRd)$. Figure 3 shows

²Throughout the paper we give the asymptotic complexity of the algorithms, assuming that each operation is executed in sequence. The methods are, however, highly amenable to parallelization, and so they can be implemented in e.g., TensorFlow very efficiently.

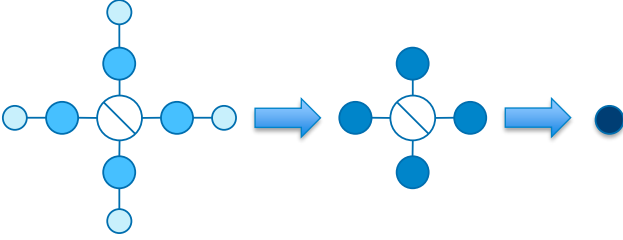


Fig. 3: Model prediction (12) in graphical TN notation, which amounts to contracting the TN in Fig. 2. The first arrow denotes matrix-vector multiplications for all factor matrices, and the second arrow the sum of Hadamard products of all resulting vectors.

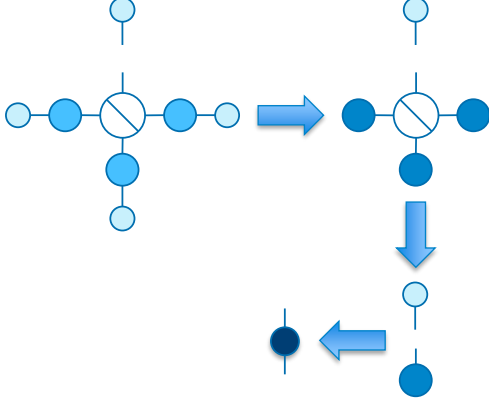


Fig. 4: Partial derivative of prediction in (12) w.r.t. a given factor matrix. The first step corresponds to matrix-vector multiplications for all but one factor matrices, the second step to the Hadamard product of the resulting vectors, and the third to the outer product of the remaining vectors.

the graphical visualization of the proposed algorithm. Notice that obtaining the model predictions amounts to contracting the TN in Fig. 2.

Algorithm 1: Model Prediction

Input: Data point $\mathbf{x} \in \mathbb{R}^N$ and factor matrices $\mathbf{A}^{(n)} \in \mathbb{R}^{d \times R}$, $1 \leq n \leq N$
Output: Prediction $\hat{y} \in \mathbb{R}$
begin
 // Construct $\phi(x_n) \in \mathbb{R}^{d \times 1}$ for $1 \leq n \leq N$
 $\mathbf{p} = \mathbf{1}^T \in \mathbb{R}^{1 \times R}$ // Initialize (row) vector of ones
 for $n = 1, \dots, N$ **do**
 | $\mathbf{p} \leftarrow \mathbf{p} \circledast \phi^T(x_n) \mathbf{A}^{(n)}$
 end
 $\hat{y} = \text{sum}(\mathbf{p})$ // Sum entries of \mathbf{p}
end

B. Learning Algorithm

In order to learn the model parameters (i.e., factor matrices) using an approach based on first-order derivatives (e.g., stochastic gradient descent, ADAM [21], etc.) we need to obtain the partial derivative of the prediction with respect to each factor matrix (the desired gradient can subsequently be

computed using the chain rule). Alternatively, one can employ automatic differentiation, for example as in Keras [22], and specify only the forward pass (i.e., Algorithm 1).

We derive this partial derivative analytically as follows, using the mode- n matricization of tensors:

$$\begin{aligned}
 f(\mathbf{x}) &= \langle \Phi(\mathbf{x}), \mathcal{W} \rangle \\
 &= \langle \Phi(\mathbf{x})_{(n)}, \mathbf{W}_{(n)} \rangle \\
 &= \text{Tr} \left(\Phi^T(\mathbf{x})_{(n)} \mathbf{W}_{(n)} \right) \\
 &= \text{Tr} \left(\left(\begin{array}{c} 1 \\ \circlearrowleft \\ \phi(x_k) \\ \circlearrowright \\ k=1 \\ k \neq n \end{array} \right) \phi^T(x_n) \mathbf{A}^{(n)} \left(\begin{array}{c} 1 \\ \circlearrowleft \\ \mathbf{A}^{(k)} \\ \circlearrowright \\ k=1 \\ k \neq n \end{array} \right)^T \right) \\
 &= \text{Tr} \left(\mathbf{A}^{(n)} \left(\begin{array}{c} 1 \\ \circlearrowleft \\ \mathbf{A}^{(k)} \\ \circlearrowright \\ k=1 \\ k \neq n \end{array} \right)^T \left(\begin{array}{c} 1 \\ \circlearrowleft \\ \phi(x_k) \\ \circlearrowright \\ k=1 \\ k \neq n \end{array} \right) \phi^T(x_n) \right) \\
 &= \text{Tr} \left(\mathbf{A}^{(n)} \left(\begin{array}{c} N \\ \circlearrowleft \\ \mathbf{A}^{(k)T} \phi(x_k) \\ \circlearrowright \\ k=1 \\ k \neq n \end{array} \right) \phi^T(x_n) \right), \quad (13)
 \end{aligned}$$

where $\text{Tr}(\cdot)$ denotes the trace operator and we have used its cyclic property.

The partial derivative of the prediction w.r.t. the n^{th} factor matrix $\mathbf{A}^{(n)}$ is then given by

$$\frac{\partial f(\mathbf{x})}{\partial \mathbf{A}^{(n)}} = \phi(x_n) \left(\begin{array}{c} N \\ \circlearrowleft \\ \mathbf{A}^{(k)T} \phi(x_k) \\ \circlearrowright \\ k=1 \\ k \neq n \end{array} \right), \quad (14)$$

where we have used the well-known matrix calculus rule

$$\frac{\partial}{\partial \mathbf{X}} \text{Tr}(\mathbf{X}\mathbf{W}) = \mathbf{W}^T. \quad (15)$$

The corresponding procedure is depicted in graphical notation in Fig. 4. Notice that a naive implementation of (14) could lead to a computational complexity of $\mathcal{O}(NRd)$ for obtaining the partial derivative w.r.t. each factor matrix and thus, a total of $\mathcal{O}(N^2Rd)$ w.r.t. to all factors. The quadratic scaling with N is due to the repetition of the same matrix-vector products as we take the derivative w.r.t. different factors, which can be obviated by storing these products. This leads to Algorithm 2, which has a complexity of $\mathcal{O}(NRd)$.

VI. LOCAL FEATURE MAPPINGS

A. Polynomial Mapping

For generality, we here consider features maps of the form

$$\phi_d(x_n) = [1, x_n, x_n^2, \dots, x_n^{(d-1)}]^T, \quad (16)$$

which are an extension to the map used in Exponential Machines [13], i.e., $\phi_{\text{EM}}(x_n) = [1, x_n]^T$. The subscript in (16) is used to emphasize the dependence on the local feature dimension d . It is important to notice that (16)

- contains the linear model (see Section VIII);

Algorithm 2: Partial Derivative of Prediction

Input: Data point $\mathbf{x} \in \mathbb{R}^N$ and factor matrices $\mathbf{A}^{(n)} \in \mathbb{R}^{d \times R}$, $1 \leq n \leq N$

Output: Partial derivative $\frac{\partial f(\mathbf{x})}{\partial \mathbf{A}^{(n)}} \in \mathbb{R}^{d \times R}$ for $1 \leq n \leq N$

begin

// Construct $\phi(x_n) \in \mathbb{R}^{d \times 1}$ for $1 \leq n \leq N$

$\mathbf{p} = \mathbf{1}^T \in \mathbb{R}^{1 \times R}$ // Initialize (row) vector of ones

for $n = 1, \dots, N$ **do**

$\mathbf{m}_n = \phi^T(x_n)\mathbf{A}^{(n)} \in \mathbb{R}^{1 \times R}$ // Store matrix-vector products

$\mathbf{p} \leftarrow \mathbf{p} \circledast \mathbf{m}_n$ // Store Hadamard products

end

for $n = 1, \dots, N$ **do**

$\mathbf{d} = \mathbf{p} \oslash \mathbf{m}_n \in \mathbb{R}^{1 \times R}$ // Divide element-wise

$\frac{\partial f(\mathbf{x})}{\partial \mathbf{A}^{(n)}} = \phi(x_n)\mathbf{d}$

end

end

- does not restrict the set of feature standardization techniques that can be employed (see Remark 1);
- and allows for the straightforward modification of d , which gives us an additional way (aside from the rank R) to vary the expressiveness of the model.

B. Normalized Polynomial Mapping

For a high enough d , the feature map in (16) causes instability in the training process and very high overfitting, especially in the presence of outliers. One solution to this issue is through normalization, and normalizing the resulting vector to unit length enables us to use a very high d , even $d > 100$, without numerical issues. As shown in Section X, such a normalization leads to a significantly better performance in the experiments conducted.

The proposed normalized map can be expressed as

$$\hat{\phi}_d(x_n) = \frac{1}{\sqrt{\sum_{k=0}^{d-1} x_n^{2k}}} [1, x_n, x_n^2, \dots, x_n^{(d-1)}]^T. \quad (17)$$

Note that, due to the dependence of the denominator on the feature values, a bias term is no longer present. Should we desire to involve bias, this may be achieved by e.g., including a unit element as the first element of the vector in (17), or simply by considering a bias with an independent parameter; we achieved best performance in our experiments by simply using (17).

As is customary in data analytics, the data are pre-processed by standardizing the features; otherwise, increasing d would quickly result in numerical overflow. We found in our experiments that standardizing to a standard deviation of 1 and mean of 0 worked well. These parameters imply that almost all feature values range between -3 and 3 after this preprocessing step, and so even $d = 75$ does not cause overflow for a 32-bit single-precision floating-point representation (one can use double-point precision for extremely high d). Furthermore, the entries of the vector in (17) either decrease exponentially with the index if the standardized feature values are between

-1 and 1, or increase exponentially otherwise. Hence, only a few of the vector entries have a non-negligible impact on the prediction.

The normalized map facilitates stability of the algorithm and smoothness of the learning curves (as seen in Section X). To gain intuition on why this is the case, we obtain an upper bound on the Frobenius norm of the partial derivative of the prediction w.r.t. each factor matrix when $\|\phi(x_n)\| = 1$:

$$\begin{aligned} \left\| \frac{\partial f(\mathbf{x})}{\partial \mathbf{A}^{(n)}} \right\| &\leq \left\| \bigotimes_{\substack{k=1 \\ k \neq n}}^N \phi^T(x_k)\mathbf{A}^{(k)} \right\| \leq \prod_{\substack{k=1 \\ k \neq n}}^N \left\| \phi^T(x_k)\mathbf{A}^{(k)} \right\| \\ &\leq \prod_{\substack{k=1 \\ k \neq n}}^N \left\| \mathbf{A}^{(k)} \right\|. \end{aligned} \quad (18)$$

Therefore, this norm is upper bounded by a value that does not depend on $\phi(x_n)$. Since the absolute value of the prediction $f(\mathbf{x})$ is bounded in a similar way, each step of gradient descent (when using e.g., mean squared error as the loss function) is also bounded. Constraining the norm of $\phi(x_n)$ prevents very large steps that could otherwise occur with high d and feature values greater than 1.

C. Mapping for Categorical Data

An advantage of the proposed framework for supervised learning is its ability to handle categorical features after they have been one-hot encoded. Although it is possible to concatenate all binary one-hot features into a large feature vector and allocate a factor matrix to each feature, thereby enabling the use of (16) with $d = 2$, this would unnecessarily model interactions between one-hot features belonging to the same categorical variable. To this end, as was done in [13], we employ the feature map for categorical data given by

$$\phi(x_n) = \left[\mathbf{1}, \mathbf{v}_n^T \right]^T, \quad (19)$$

where $\mathbf{v}_n \in \mathbb{R}^{K_n}$ is the one-hot-encoded representation of the n^{th} categorical feature, and K_n is the number of values that the feature can assume.

Remark 1. A feature map in [12], [23], given by $\phi(x_n) = \left[\cos\left(\frac{\pi}{2}x_n\right), \sin\left(\frac{\pi}{2}x_n\right) \right]^T$, was inspired by quantum physics and has been used for object recognition tasks. A potential issue with this map for other types of tasks is that \cos and \sin are one-to-one functions only if their domains are restricted. Thus, if the input features are unbounded (i.e., there are no pre-defined minimum and maximum values), it is only possible to apply Min-Max scaling (and not other standardization techniques) to the features as a preprocessing step. Although pixel values in images are bounded (typically from 0 to 255), this is not normally the case for other data types. This is particularly problematic in the presence of outliers, as, in that case, Min-Max scaling can result in extremely small standard deviations for the scaled features, and in an adverse impact on the performance.

VII. REGULARIZATION

Although the CP decomposition itself provides strong regularization for small rank³, there is room to improve the performance by guiding the training algorithm to hypotheses that are more likely to generalize well for unseen data. However, standard regularizers, such as through L1 and L2 norms, do not differentiate between the coefficients for different feature interactions in (11). This is likely to prove suboptimal when using the polynomial or categorical mappings, as often the application dictates to constrain the coefficients of the higher-order terms relatively more. *Order regularization* [13] addresses this issue by penalizing large coefficients for higher-order terms more than those for lower-order ones. We now proceed to employ order regularization in our model.

The penalty for order regularization is given by $\langle \mathcal{B} \circledast \mathcal{W}, \mathcal{B} \circledast \mathcal{W} \rangle$, where $\mathcal{B} = \bigcirc_{k=1}^N \mathbf{b}$ for a user-defined vector \mathbf{b} . In the case of polynomial functions, one choice is $\mathbf{b} = [1, \beta, \beta^2, \dots, \beta^{d-1}]^T$ with $\beta > 1$. In other words, the coefficients of the higher-order terms are multiplied by a higher power of β in the computation of the penalty function, and the factor matrices are adjusted in such a way so as to shrink these coefficients relatively more. In the case of categorical feature mapping, $\mathbf{b} = [1, \beta, \beta, \dots, \beta]^T$ is more suitable, since all binary, one-hot features should be treated equally.

A. Computation of the Order Regularization Penalty

A closer inspection of the term $\mathcal{B} \circledast \mathcal{W}$ gives

$$\begin{aligned} \mathcal{B} \circledast \mathcal{W} &= \left(\bigcirc_{k=1}^N \mathbf{b} \right) \circledast \left(\sum_{r=1}^R \bigcirc_{k=1}^N \mathbf{a}_r^{(k)} \right) \\ &= \sum_{r=1}^R \bigcirc_{k=1}^N \left(\mathbf{a}_r^{(k)} \circledast \mathbf{b} \right). \end{aligned} \quad (20)$$

Now, let $\mathbf{B} = [\mathbf{b}, \dots, \mathbf{b}] \in \mathbb{R}^{d \times R}$ and $\mathbf{Y}^{(n)} = \mathbf{A}^{(n)} \circledast \mathbf{B}$. The penalty $\langle \mathcal{B} \circledast \mathcal{W}, \mathcal{B} \circledast \mathcal{W} \rangle$ can now be re-written as

$$\begin{aligned} P(\mathcal{B}, \mathcal{W}) &= \text{vec}(\mathcal{B} \circledast \mathcal{W})^T \text{vec}(\mathcal{B} \circledast \mathcal{W}) \\ &= \mathbf{1}^T \left(\begin{array}{c} 1 \\ \circlearrowleft \\ \mathbf{Y}^{(k)} \\ \hline \mathbf{Y}^{(k)} \\ \circlearrowleft \\ 1 \end{array} \right)^T \left(\begin{array}{c} 1 \\ \circlearrowleft \\ \mathbf{Y}^{(k)} \\ \hline \mathbf{Y}^{(k)} \\ \circlearrowleft \\ 1 \end{array} \right) \mathbf{1} \\ &= \mathbf{1}^T \left(\begin{array}{c} N \\ \circlearrowleft \\ \mathbf{Y}^{(k)T} \mathbf{Y}^{(k)} \\ \hline \mathbf{Y}^{(k)T} \mathbf{Y}^{(k)} \\ \circlearrowleft \\ N \end{array} \right) \mathbf{1}. \end{aligned} \quad (21)$$

The procedure for computing the regularization penalty is given in Algorithm 3 and depicted graphically in Fig. 5. The algorithm has a computational cost of $\mathcal{O}(NR^2d)$, so that the training procedure now scales quadratically in R with order regularization (rather than linearly as before).

³The main assumption is that the true matrices we aim to approximate lie near some low-dimensional subspaces.

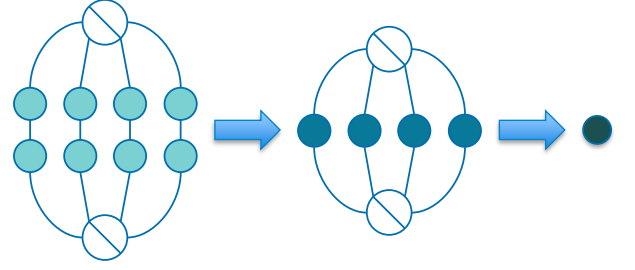


Fig. 5: Order regularization penalty in graphical TN notation for $N = 4$. The first arrow denotes matrix-matrix multiplications for all factor matrices and second arrow designates the sum of Hadamard products of all resulting matrices. Note that the matrices in the left-most TN result from the Hadamard products $\mathbf{A}^{(n)} \circledast \mathbf{B}$.

Algorithm 3: Order Regularization Penalty

Input: Factor matrices $\mathbf{A}^{(n)} \in \mathbb{R}^{d \times R}$, $1 \leq n \leq N$, order regularization parameter $\mathbf{b} \in \mathbb{R}^{d \times 1}$, and regularization constant $\alpha \in \mathbb{R}$

Output: Penalty $P \in \mathbb{R}$

begin

$\mathbf{B} = [\mathbf{b}, \dots, \mathbf{b}]^T \in \mathbb{R}^{d \times R}$

$\mathbf{P} = [\mathbf{1}, \dots, \mathbf{1}]^T \in \mathbb{R}^{R \times R}$ // Initialize all-ones matrix

for $n = 1, \dots, N$ **do**

$\mathbf{P} \leftarrow \mathbf{P} \circledast \left(\left(\mathbf{A}^{(n)} \circledast \mathbf{B} \right)^T \left(\mathbf{A}^{(n)} \circledast \mathbf{B} \right) \right)$

end

$P = \alpha * \text{sum}(\mathbf{P})$ // Sum entries of \mathbf{P}

end

B. Partial Derivative of the Order Regularization Penalty

The partial derivative of the order regularization penalty w.r.t. each factor matrix can be found by first expressing the penalty in the following way:

$$\begin{aligned} P &= \left\langle \left(\mathbf{B}_{(n)} \circledast \mathbf{W}_{(n)} \right), \left(\mathbf{B}_{(n)} \circledast \mathbf{W}_{(n)} \right) \right\rangle \\ &= \text{Tr} \left(\left(\mathbf{B}_{(n)} \circledast \mathbf{W}_{(n)} \right)^T \left(\mathbf{B}_{(n)} \circledast \mathbf{W}_{(n)} \right) \right) \\ &= \text{Tr} \left(\left(\begin{array}{c} 1 \\ \circlearrowleft \\ \mathbf{Y}^{(k)} \\ \hline \mathbf{Y}^{(k)} \\ \circlearrowleft \end{array} \right) \mathbf{Y}^{(n)T} \mathbf{Y}^{(n)} \left(\begin{array}{c} 1 \\ \circlearrowleft \\ \mathbf{Y}^{(k)} \\ \hline \mathbf{Y}^{(k)} \\ \circlearrowleft \end{array} \right)^T \right) \\ &= \text{Tr} \left(\mathbf{Y}^{(n)} \left(\begin{array}{c} 1 \\ \circlearrowleft \\ \mathbf{Y}^{(k)} \\ \hline \mathbf{Y}^{(k)} \\ \circlearrowleft \end{array} \right)^T \left(\begin{array}{c} 1 \\ \circlearrowleft \\ \mathbf{Y}^{(k)} \\ \hline \mathbf{Y}^{(k)} \\ \circlearrowleft \end{array} \right) \mathbf{Y}^{(n)T} \right) \\ &= \text{Tr} \left(\mathbf{Y}^{(n)} \left(\begin{array}{c} N \\ \circlearrowleft \\ \mathbf{Y}^{(k)T} \mathbf{Y}^{(k)} \\ \hline \mathbf{Y}^{(k)T} \mathbf{Y}^{(k)} \\ \circlearrowleft \end{array} \right) \mathbf{Y}^{(n)T} \right). \end{aligned} \quad (22)$$

Then, using the identity (see Appendix B for proof)

$$\frac{\partial}{\partial \mathbf{X}} \text{Tr} \left((\mathbf{X} \circledast \mathbf{W}) \mathbf{Z} (\mathbf{X} \circledast \mathbf{W})^T \right) = \mathbf{W} \circledast \left((\mathbf{X} \circledast \mathbf{W}) (\mathbf{Z} + \mathbf{Z}^T) \right) \quad (23)$$

we arrive at (notice that in this case $\mathbf{Z} = \mathbf{Z}^T$)

$$\frac{\partial P}{\partial \mathbf{A}^{(n)}} = 2\mathbf{B} \circledast \left(\mathbf{Y}^{(n)} \left(\bigotimes_{\substack{k=1 \\ k \neq n}}^N \mathbf{Y}^{(k)T} \mathbf{Y}^{(k)} \right) \right). \quad (24)$$

As in Algorithm 2, by storing the Hadamard products, the procedure for computing the partial derivative of the penalty w.r.t. all factor matrices scales linearly with N rather than quadratically, leading to a time complexity of $\mathcal{O}(NR^2d)$ (see Algorithm 4); the corresponding memory complexity is $\mathcal{O}(NRd + R^2)$. To further speed up the algorithm, it is possible to store the matrix products $(\mathbf{A}^{(n)} \circledast \mathbf{B})^T (\mathbf{A}^{(n)} \circledast \mathbf{B})$ in the first `for` loop to avoid computing them in the second one. This, however, would have no effect on the asymptotic computational complexity and would increase the memory complexity to $\mathcal{O}(NRd + NR^2)$.

Algorithm 4: Partial Derivative of Order Regularization Penalty

Input: Factor matrices $\mathbf{A}^{(n)} \in \mathbb{R}^{d \times R}$, $1 \leq n \leq N$, order regularization parameter $\mathbf{b} \in \mathbb{R}^{d \times 1}$, and regularization coefficient $\alpha \in \mathbb{R}$

Output: Partial derivative $\frac{\partial P}{\partial \mathbf{A}^{(n)}} \in \mathbb{R}^{d \times R}$ for $1 \leq n \leq N$
begin

$\mathbf{B} = [\mathbf{b}, \dots, \mathbf{b}]^T \in \mathbb{R}^{d \times R}$
 $\mathbf{P} = [\mathbf{1}, \dots, \mathbf{1}]^T \in \mathbb{R}^{R \times R}$ // Initialize all-ones matrix
for $n = 1, \dots, N$ **do**
 $\mathbf{P} \leftarrow \mathbf{P} \circledast \left((\mathbf{A}^{(n)} \circledast \mathbf{B})^T (\mathbf{A}^{(n)} \circledast \mathbf{B}) \right)$ // Store Hadamard products

end
for $n = 1, \dots, N$ **do**
 $\mathbf{D} = \mathbf{P} \oslash \left((\mathbf{A}^{(n)} \circledast \mathbf{B})^T (\mathbf{A}^{(n)} \circledast \mathbf{B}) \right) \in \mathbb{R}^{R \times R}$
 // Divide element-wise
 $\frac{\partial P}{\partial \mathbf{A}^{(n)}} = 2\alpha \mathbf{B} \circledast \left((\mathbf{A}^{(n)} \circledast \mathbf{B}) \mathbf{D} \right)$

end
end

VIII. INITIALIZATION OF FACTOR MATRICES

One way to initialize the factor matrices is to use independent zero-mean Gaussian noise, with a tunable standard deviation. However, if the local feature map is of the form $\phi(x_n) = [1, \psi^{(1)}(x_n), \dots, \psi^{(d-1)}(x_n)]^T$, where $\psi^{(j)}: \mathbb{R} \rightarrow \mathbb{R}$, it is possible to initialize the factors matrices by employing the solution of a linear model (linear or logistic regression depending on the task), trained on the set of features

$\{\psi^{(j)}(x_n) \mid 1 \leq j \leq d-1, 1 \leq n \leq N\}$. Note that the linear model can also be trained on a subset of this set, as is performed in Example 4, but for clarity we assume for now the full set of transformed features.

Let b denote the bias term of the linear model trained on the aforementioned set; in addition, let $w_{n,j}$ denote its weight corresponding to the n^{th} feature and the function $\psi^{(j)}$. Then, the CP-based model produces the same predictions as the linear model if the entries of the factor matrices are given by

$$a_{1,r}^{(n)} = \begin{cases} \frac{b}{N}, & \text{for } r = n \\ 1, & \text{for } 1 \leq r \leq N, r \neq n, \\ 0 & \text{otherwise} \end{cases} \quad (25)$$

$$a_{j,r}^{(n)} = \begin{cases} w_{r,j-1}, & \text{for } r = n, j = 2, \dots, d \\ 0 & \text{otherwise} \end{cases}$$

With such an initialization, the error at the first epoch tends to be lower than with random initialization and sometimes also converges to a lower value. This is especially common when the number of features is high (e.g., larger than 20).

To prove that the initialization indeed yields the same prediction as the linear model, notice from (11) that the bias term for the CP-based model is obtained through the sum of the Hadamard products of the first rows of the factor matrices, to give

$$\left(\bigotimes_{k=1}^N \hat{\mathbf{a}}_1^{(k)} \right) \mathbf{1} = \left[\underbrace{\left[\frac{b}{N}, \dots, \frac{b}{N} \right]}_{N \text{ times}}, 0, \dots, 0 \right] \mathbf{1} = b. \quad (26)$$

Moreover, the coefficient for $\psi_j(x_n)$ is obtained as

$$\left(\bigotimes_{\substack{k=1 \\ k \neq n}}^N \hat{\mathbf{a}}_1^{(k)} \circledast \hat{\mathbf{a}}_{j+1}^{(n)} \right) \mathbf{1} = \left(\left[\underbrace{\left[\frac{b}{N}, \dots, \frac{b}{N} \right]}_{n-1 \text{ times}}, 1, \underbrace{\left[\frac{b}{N}, \dots, \frac{b}{N} \right]}_{N-n \text{ times}}, 0, \dots, 0 \right] \circledast \underbrace{\left[0, \dots, 0, w_{n,j}, 0, \dots, 0 \right]}_{n-1 \text{ times}} \right) \mathbf{1} = w_{n,j}. \quad (27)$$

while the coefficient for the second-order interaction $\psi_q(x_l)\psi_r(x_m)$ for $1 \leq q, r \leq d-1$, $1 \leq l, m \leq N$, and $l \neq m$ becomes

$$\left(\bigotimes_{\substack{k=1 \\ k \neq l \\ k \neq m}}^N \hat{\mathbf{a}}_1^{(k)} \circledast \hat{\mathbf{a}}_{q+1}^{(l)} \circledast \hat{\mathbf{a}}_{r+1}^{(m)} \right) \mathbf{1} = 0 \quad (28)$$

since $\hat{\mathbf{a}}_{q+1}^{(l)} \circledast \hat{\mathbf{a}}_{r+1}^{(m)} = \mathbf{0}$ for all l, m , $l \neq m$ and all q, m . Finally, in the same spirit, it is obvious that the coefficients of the higher-order interactions are also 0.

Example 4. A consequence of (25) is that the CP-based model with the polynomial feature map given in (16) inherently contains the solution of the linear model trained on the original features. Namely, given the coefficient for the n^{th}

feature w_n , the relevant initialization for the entries of the factor matrices is given by

$$a_{1,r}^{(n)} = \begin{cases} \frac{b}{N}, & \text{for } r = n \\ 1, & \text{for } 1 \leq r \leq N, r \neq n, \\ 0 & \text{otherwise} \end{cases}$$

$$a_{2,r}^{(n)} = \begin{cases} w_n, & \text{for } r = n \\ 0 & \text{otherwise} \end{cases} \quad (29)$$

and all other rows equal $\mathbf{0}$, since they correspond to features raised to higher powers than 1.

Remark 2. When dealing with categorical features that are one-hot encoded, the initialization changes slightly due to the fact that the number of rows of the factor matrices is not constant (see Section VI). Given N categorical features, each assuming K_n ($1 \leq n \leq N$) values, the rows of the factor matrices can be initialized as in (25), except that d must be replaced with K_n . Note that in this case, $w_{n,j}$ denotes the weight of the binary feature corresponding to the n^{th} categorical feature and its j^{th} possible value.

IX. RELATED WORK

In this section, we discuss similarities and differences between the proposed CP-based model and related works.

A. TT-based Models

The work in [12] and [13] both used the TT format to reduce the number of model parameters. The former proposed an algorithm inspired from quantum physics that allows the adaptation of the TT rank during training; unfortunately, it scales cubically with the local dimension d . The authors of [13] designed a stochastic version of a Riemannian optimization approach, which they found to be more robust to initialization than stochastic gradient descent methods. In terms of the local feature mappings, both works used $d = 2$ (see Section VI).

To better understand how the TT-based models are linked to the CP-based one, it is important to notice that a CP decomposition can be expressed in terms of the TT format. Specifically, a tensor in the CP format with rank R is equivalent to a tensor in the TT format, for which the TT cores are given by $\mathcal{G}^{(1)} = \mathbf{A}^{(1)}$, $\mathcal{G}^{(N)} = \mathbf{A}^{(N)T}$, and $\mathbf{G}_{i_n}^{(n)} = \text{diag}(a_{i_n,1}, \dots, a_{i_n,R})$ for $n = 2, \dots, N - 1$, where $\mathbf{G}_{i_n}^{(n)}$ are the lateral slices of the cores [24]. Hence, any CP-decomposed weight tensor can be converted into its TT format. However, the predictions produced by the models are not equivalent, since an optimization process on the TT-based model alters the off-diagonal terms of the core tensors, i.e., they are not constrained to be zero. Thus, the differences in performance between the two models arise due to off-diagonal core elements being either helpful or detrimental to the generalization capabilities for the dataset at hand. Viewed another way, for an equal number of parameters, the TT-based model will achieve superior results if and only if it is better for generalization to have TT cores whose slices are relatively small matrices with off-diagonal terms rather than larger diagonal matrices. Note also that any tensor in

the TT format can be mapped to a tensor in the CP format, but, in general, the CP rank equals $R_1 R_2 \cdots R_{N-1}$, while TT rank = $\{R_1, \dots, R_{N-1}\}$ [24].

A potential advantage of the CP-based model for non-sequential data is its insensitivity to the ordering of the features, as, when constrained to be laterally diagonal, the cores can be permuted in any way without altering the decomposition (since diagonal matrices commute). On the other hand, the TT-based models may be more suitable for sequential data due to the inherent ordering of their cores.

B. Kernel SVM

The CP-based model with a polynomial feature map resembles an SVM with the polynomial kernel, the prediction of which is given by

$$\hat{y}(\mathbf{x}) = \langle \psi(\mathbf{x}), \mathbf{w}_{\text{svm}} \rangle, \quad (30)$$

where ψ maps the feature vector \mathbf{x} onto a higher-dimensional space, and \mathbf{w}_{svm} are the parameters of the SVM model. Recall that an SVM with a polynomial kernel, $K(\mathbf{x}, \mathbf{z}) = \langle \psi(\mathbf{x}), \psi(\mathbf{z}) \rangle = (\langle \mathbf{x}, \mathbf{z} \rangle + 1)^i$, can model an i^{th} -degree polynomial, similarly to our model (with $d = i + 1$). However, the disadvantages of the polynomial SVM compared to the CP-based model, are:

- at least quadratic scaling with the training set size;
- tendency to overfit for large i , since, unlike our model, the SVM parameters are independent of one another;
- inability to effectively capture interactions for sparse (categorical) data (e.g., recommender systems);
- compromised interpretability since one cannot recover the coefficients of the polynomial;
- predictions depending on the training data, or support vectors.

C. Higher-Order Factorization Machines and Polynomial Networks

Higher-Order Factorization Machines (HOFM) [25] address the limitations of the SVMs by factorizing the interaction parameters. The order in this case refers to the highest degree of feature interactions being modelled (e.g., an order of three refers to modelling interactions containing a maximum of three variables). Although a HOFM resembles the CP-based model when $\phi(x_n) = [1, x_n]^T$, there are some important differences, which can be illuminated by casting HOFM into the tensor format [26].

A HOFM of order L can be expressed in the tensor format as

$$\hat{y} = \sum_{l=1}^L \sum_{j_1 > \dots > j_l} \hat{w}_{j_1, \dots, j_l}^{(l)} \prod_{k=1}^l x_{j_k}, \quad (31)$$

where the weight tensors $\hat{W}^{(l)} \in \mathbb{R}^{N_l}$ ($l = 1, \dots, L$) are represented in the *symmetric* CP format. Furthermore, in this formulation we observe the outer product of the whole feature vector \mathbf{x} with itself L times. Finally, only the entries above the super-diagonal of the weight tensors (which correspond to the products of distinct features) are used to construct the output.

In contrast, the proposed CP-based model takes the inner product between a tensor assumed to be in the (asymmetric) CP format (and of order equal to the number of features) and a tensor formed from the outer product of the local feature maps $\phi(x_n) = [1, x_n]^T$.

Similarly, Polynomial Networks (PN) [27] can be cast to the form [26]:

$$\hat{y} = \sum_{l=1}^L \sum_{j_1, \dots, j_l} \hat{w}_{j_1, \dots, j_l}^{(l)} \prod_{k=1}^l x_{j_k}, \quad (32)$$

with the difference from (31) in the subscript of the second sum; this is related to our model when $\phi(x) = [1, x, x^2, \dots, x^{(d-1)}]^T$ in the same way as described for HOFM.

Unlike HOFM and PN, the CP-model used in our work allows for the modelling of all-order interactions with a computational complexity that scales linearly with the number of features during both training and inference.

D. Convolutional Arithmetic Circuits

The CP-based model can be viewed as a special case of the model presented in [6] (see Section 3 in [6]), where a data instance is represented as a collection of vectors, each of dimensionality s . In the case of a grayscale image, these vectors may correspond to s consecutive pixels. The so-called representation functions (analogous to the local feature maps) are then applied on each of these vectors, using for example an affine transformation followed by an activation function. This model is referred to in [6] as the Convolutional Arithmetic Circuit due to the nature of the representation function. The main differences between the CP-based model and the model presented in [6] are that we use $s = 1$ and the representation functions that we apply are those given in Section VI.

It was proved in [6] that a model based on the Hierarchical Tucker (HT) decomposition is exponentially more expressive than that based on CP; that is, an HT-based model realizes functions that would almost always require a CP-based model with an exponentially large rank to even approximate them. A similar result was proved in [7], where a model based on CP was compared with one based on TT. Although this may at first appear as a disadvantage of the CP-based model, we argue that this is not so, at least for non-sequential data. The model architecture captures an inductive bias about the task at hand, and due to either potential overfitting or optimization difficulties, a model that is more expressive than necessary is likely to converge to a solution that is inferior to that obtained by a model well-suited to the data. Our experiments on non-sequential data comparing CP- and TT-based models confirm this hypothesis. We also show that increasing the rank did not significantly improve the validation loss, which is further empirical evidence that it is unlikely that the target function for these tasks is one that the CP-based model needs an exponentially large rank to approximate.

X. EXPERIMENTS

To demonstrate the generality and flexibility of the proposed approach, comprehensive experiments were performed over three case studies of different nature:

- a synthetic polynomial regression task, that illustrates the effects of initialization from the linear model solution and order regularization, for lower than and higher than optimal local dimensions;
- MovieLens 100K recommender system dataset (classification on very sparse categorical data);
- the benchmark California Housing dataset (regression with many outliers), to show the utility of using very high local dimension, coupled with normalized polynomial feature mappings.

The MovieLens and California housing datasets were chosen as illustrative examples of very common tasks in machine learning.

The performance of our model was evaluated against the TT-based model as well as other common supervised learning models. For the former, we used the code provided in Google’s TensorNetwork library [28]. Moreover, we used the `scikit-learn` implementation of the SVM and the Keras library to construct the neural networks, as well as `polylearn`⁴ and `tffm`⁵ for the Polynomial Networks and Higher-Order Factorization Machines, respectively.

A. Effects of Initialization and Order Regularization

For this experiment, a synthetic dataset was used, with the target function set to a 2nd-order polynomial of 3,000 samples of four features with added white Gaussian noise, and the models were trained on seven features, i.e., three of the features were non-informative. We used the (unnormalized) polynomial map, so that the target function was included in the hypotheses sets of the CP- and TT-based models (for $d \geq 3$). As a preprocessing step, the features were standardized to zero mean and unit variance, and the mean squared error (MSE) was used as the loss function. Moreover, for the iterative methods, the mini-batch size was set to 32, and the ADAM optimizer was used. The neural network was composed of three hidden layers, with 20 neurons for the first two and 15 for the last layer, all followed by the ReLu activation and batch normalization [29]. The test set comprised 20% of the dataset, while 20% of the remaining data points formed the validation set.

Fig. 6 shows the influence of linear initialization and order regularization on the proposed model for different local dimensions, with the neural network acting as a baseline. Specifically, we trained the models over 60 epochs, first with random initialization (zero-mean Gaussian noise with standard deviation of 0.2) and no regularization, then with the linear model solution as initialization, and finally order regularization was included with $\beta = 3.0$ and $\alpha = 10^{-3}$. The top panel of Figure 6 shows the learning curves for $d = 2$ and $R = 7$, and illustrates that the model was not expressive enough to capture the 2nd-order terms of the polynomial. Despite the linear-initialized model starting from a significantly lower validation error and converging faster, both initialization schemes led to the model reaching the same error after 4-5 epochs; the neural network converged after about 60 epochs to a similar

⁴<https://github.com/scikit-learn-contrib/polylearn>

⁵<https://github.com/geffy/tffm>

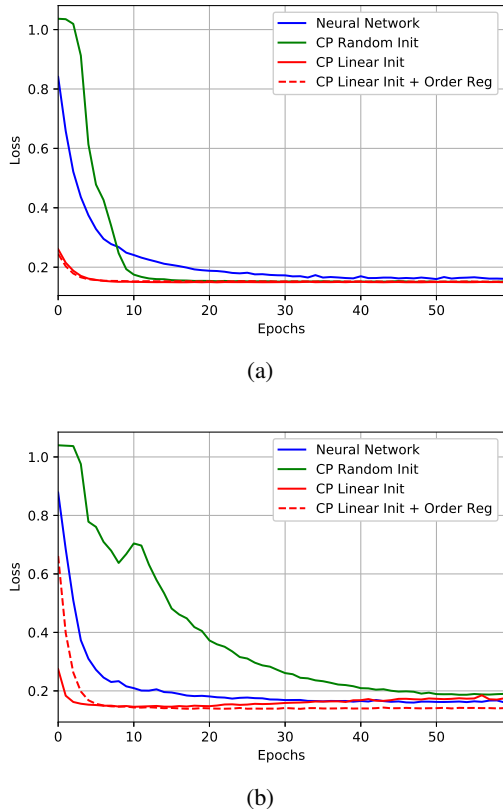


Fig. 6: Learning curves of validation MSE for the synthetic polynomial regression task. The effects of initialization with the linear model solution and order regularization are shown for (a) smaller local dimension than the optimal ($d = 2$) and $R = 7$, and (b) larger local dimension than the optimal ($d = 4$) and $R = 30$.

TABLE I: Validation losses and training times for the synthetic regression dataset.

Method	Val Loss	Train Time (sec)
CP-Based ($d = 3$)	0.1378	11.09
Linear Regression	0.3311	0.004
RBF SVR	0.1790	1.30
Neural Network	0.1545	20.59
3 rd -order Polynomial Network	0.1390	6.96
3 rd -order Factorization Machine	0.1485	4.35

value. Also, order regularization did not have a significant effect on the performance of the model. On the other hand, when d was increased to four (a higher than optimal local dimension, as there were no 3rd-order terms) and R to 30, the random initialization scheme took significantly longer to converge (around 60 epochs, then it started overfitting), and order regularization enabled the optimization procedure to reach a lower validation error.

A comparison with the other models considered is given in Table I, which shows the minimum validation score across 100 epochs and training times. We were not able to run the TT-based models with the unnormalized polynomial mapping (neither Google’s TensorNetwork nor Exponential Machines with $d = 2$), as the loss diverged with all hyperparameters we tried.

B. Performance on Recommender System

Categorical data cause issues to traditional neural networks and SVMs due to data sparsity after one-hot encoding. For example, SVMs with a polynomial kernel find it difficult to learn the coefficients corresponding to interactions of two or more categorical features, because there are usually not enough training points where the relevant binary, one-hot features are both “hot.” In contrast, the CP-based model factorizes these coefficients and, thus, performs well in such settings (for a detailed discussion on why factorized models perform well with sparse data see [25]).

We next demonstrate the performance of our model on the MovieLens 100K, a widely-used benchmark for sparse data classification; for more details see [30]. For the preprocessing of the data, we followed the procedure described in [13], in order to be able to directly compare the results with the TT-based model (Exponential Machines). The features were mapped as described in Section VI-C. The CP rank was set to 30, and order regularization was added with $\beta = 3.6$ and $\alpha = 5 \times 10^{-5}$, respectively. We trained the model until convergence, obtaining an Area Under Curve (AUC) score of **0.7863**, which is higher than that in original Exponential Machines work which reported an AUC score of 0.784. Note that logistic regression obtained a score of 0.7821. For a comparison with other models, we refer the reader to [13]. We found that both initialization from the linear model solution and order regularization helped significantly in achieving better performance on this task.

C. Effect of Local Dimension

To show the effect of high d on a common single-target regression dataset, we employed the California Housing dataset, comprising eight features and 20,640 samples, and with similar data pre-processing as for the synthetic example; the CP rank was set to 20. We found that, for the unnormalized polynomial map, increasing d from two to three improved performance, but any further increase caused the learning procedure to become highly unstable and eventually to experience numerical instability. Standardizing (zero mean, unit standard deviation) each element of the resulting vector after mapping prevented overflow but led to relatively erratic learning curves for validation (see Fig 7).

In contrast, the model with the normalized polynomial map (with random initialization⁶) was able to be trained reliably even for very high d , as indicated by the smooth learning curves in Fig. 7. In addition, without regularization the training error kept decreasing to very small values, reflecting the gains in expressiveness (see Fig. 8). The lowest validation error (without regularization) was obtained with $d = 25$, and it remained low even for dimensions around 100, indicating the regularization capabilities of low rank. Of course, with a smaller dataset, we would observe more overfitting for high d . With L2 regularization on the factor matrices, the validation error reached its smallest value at $d = 75$ (we did not observe any improvement using order regularization over L2 with this map and on this dataset).

⁶It is also possible to use initialization from the linear model.

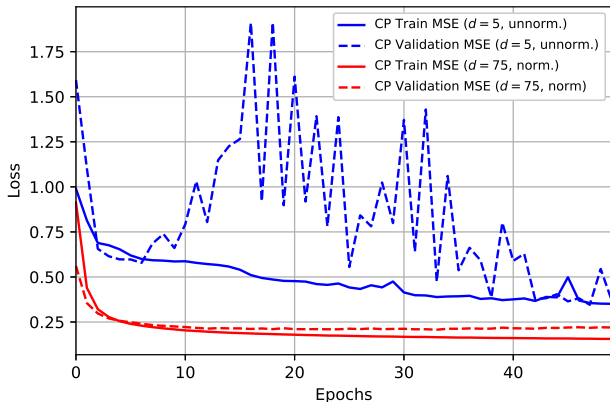


Fig. 7: Learning curves for $d = 5$ with the unnormalized polynomial map and for $d = 75$ with the normalized polynomial map.

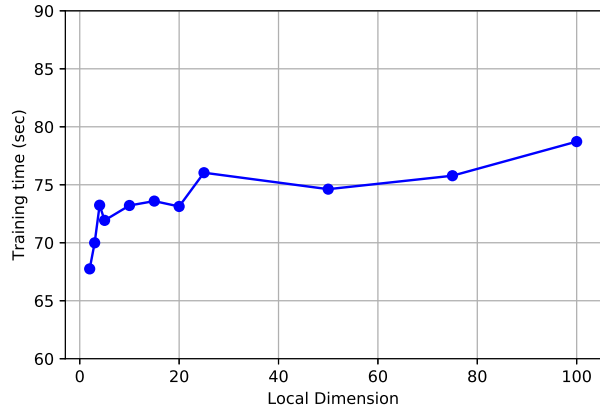


Fig. 9: Training time in seconds as a function of the local dimension (run for 50 epochs and CP rank equal to 20).

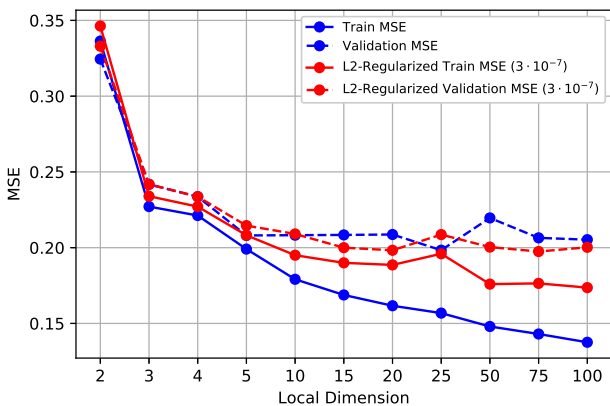


Fig. 8: Validation loss as a function of the local dimension with and without L2 regularization.

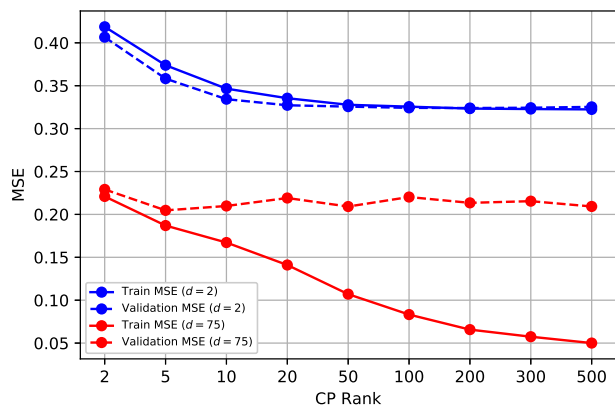


Fig. 10: Training and validation losses as functions of the CP rank for low and high local dimensions.

A higher d not only resulted in significant gains in performance, but it also had a small impact on training time, due to optimized matrix-vector multiplications in TensorFlow, enabling fast tuning of this hyperparameter (see Fig. 9).

A comparison with the other models is given in Table II. The TT rank was set to 5, leading to the same number of parameters as in the CP-based model. Note that the very large training time compared to the CP-based model is likely due to the different implementation in TensorFlow, and not due to the

TT-based model being inherently slower to train for the same number of parameters. The feedforward neural network that we constructed contained four hidden layers and also had an equal number of parameters. The minimum validation score across 100 epochs is reported.

D. Effect of CP Rank

The CP rank affects performance differently for low d than for high d . As can be seen in Fig. 10, both the training and validation errors were decreasing up to rank equal to 50 and then plateaued for $d = 2$. On the other hand, when d was increased to 75, although the training error was decreasing with higher rank, the validation error remained fairly constant. Notice that even with very small rank (about 2 to 5), the validation error still stayed significantly lower than for any value of rank with $d = 2$. This suggests that the local dimension is more important than the rank for accurate model predictions.

TABLE II: Validation losses and training times for the California Housing dataset.

Method	Val MSE	Train Time (sec)
CP-Based ($d = 2$, unnorm.)	0.3348	36.40
CP-Based ($d = 5$, unnorm.)	0.4221	41.29
CP-Based ($d = 25$, norm.)	0.2090	51.15
CP-Based ($d = 75$, norm., w/ L2)	0.1959	118.84
TT-Based ($d = 25$, norm.)	0.2139	773.25
Linear Regression	0.3712	0.023
RBF SVR	0.2236	18.78
Neural Network	0.2029	153.20
4th order Polynomial Network	0.2761	9.06
4th order Factorization Machine	0.3322	51.69

E. Effect of Large Number of Features

Increasing the number of features beyond a certain point (e.g., about 30) often makes the optimization process more sensitive to the width of the Gaussian distribution when random initialization is used. This stems from the many Hadamard products (or matrix-matrix products in the case of TT-based models) that are performed; if the standard deviation of the Gaussian is too small or too big, this can lead to vanishingly small or exceedingly large predictions (and gradients), respectively. Initialization with a linear model solution largely alleviates this issue, as was confirmed when the model was trained on the (flattened) MNIST dataset with 784 features. It would be interesting to investigate other strategies that could enable these models to achieve state-of-the-art results on very high-dimensional datasets, a subject of future work.

XI. CONCLUSION AND FUTURE WORK

We have introduced scalable inference and learning algorithms for a supervised learning model based on the Canonical Polyadic (CP) decomposition to serve as a robust and simpler alternative to the existing methods based on the Tensor Train (TT) for supervised learning non-sequential tasks. The proposed model has been shown to be applicable to both standard classification and regression tasks as well as in recommender systems. We have also derived efficient procedures to incorporate order regularization and have established a procedure for model initialization using a linear model solution. In addition, we have proposed a unit-normalized version of an arbitrarily high-dimensional local feature map, which enables the straightforward increase in model expressiveness and remains stable for very high dimensions.

Future research directions will extend the Riemannian optimization approach of Exponential Machines to handle high local dimensions for TT-based supervised learning and compare the performance with adaptive gradient approaches. It could also be fruitful to experiment with other local feature maps and establish a comparison with those considered here. Another potential line of follow-up work could be finding novel techniques to help in the training of the models when the dimensionality of the features is very high. Finally, future research could focus on the generalization ability of the models when different tensor networks (TNs) are employed to represent the weight tensor, depending on the nature of the data at hand. For example, given the inherent one-dimensional structure of natural language processing problems or the two-dimensional nature of images, it seems likely that the TT representation (1-D TNs) would lead to superior performance in the former case while PEPS [31] (2-D TNs) would be more suitable in the latter case.

APPENDIX A

PROOF OF THE KHATRI-RAO PROPERTY

We here prove the identity in (1). Let $\mathbf{A}^{(k)} \in \mathbb{R}^{I_k \times J}$ and $\mathbf{B}^{(k)} \in \mathbb{R}^{I_k \times L}$, $1 \leq k \leq N$. Since

$$\begin{aligned} \left(\bigcirc_{k=1}^N \mathbf{A}^{(k)} \right)^T &= \left[\bigotimes_{k=1}^N \mathbf{a}_1^{(k)} \quad \cdots \quad \bigotimes_{k=1}^N \mathbf{a}_J^{(k)} \right]^T, \\ \left(\bigcirc_{k=1}^N \mathbf{B}^{(k)} \right) &= \left[\bigotimes_{k=1}^N \mathbf{b}_1^{(k)} \quad \cdots \quad \bigotimes_{k=1}^N \mathbf{b}_L^{(k)} \right], \end{aligned}$$

and using the mixed-product property [32]

$$\left(\bigotimes_{k=1}^N \mathbf{a}_j^{(k)T} \right) \left(\bigotimes_{k=1}^N \mathbf{b}_j^{(k)} \right) = \bigotimes_{k=1}^N \mathbf{a}_j^{(k)T} \mathbf{b}_j^{(k)} \quad (33)$$

we obtain

$$\begin{aligned} &\left(\bigcirc_{k=1}^N \mathbf{A}^{(k)} \right)^T \left(\bigcirc_{k=1}^N \mathbf{B}^{(k)} \right) \\ &= \left[\begin{array}{ccc} \bigotimes_{k=1}^N \mathbf{a}_1^{(k)T} \mathbf{b}_1^{(k)} & \cdots & \bigotimes_{k=1}^N \mathbf{a}_1^{(k)T} \mathbf{b}_L^{(k)} \\ \vdots & \ddots & \vdots \\ \bigotimes_{k=1}^N \mathbf{a}_J^{(k)T} \mathbf{b}_1^{(k)} & \cdots & \bigotimes_{k=1}^N \mathbf{a}_J^{(k)T} \mathbf{b}_L^{(k)} \end{array} \right] \\ &= \left[\begin{array}{ccc} \prod_{k=1}^N \mathbf{a}_1^{(k)T} \mathbf{b}_1^{(k)} & \cdots & \prod_{k=1}^N \mathbf{a}_1^{(k)T} \mathbf{b}_L^{(k)} \\ \vdots & \ddots & \vdots \\ \prod_{k=1}^N \mathbf{a}_J^{(k)T} \mathbf{b}_1^{(k)} & \cdots & \prod_{k=1}^N \mathbf{a}_J^{(k)T} \mathbf{b}_L^{(k)} \end{array} \right] \\ &= \bigotimes_{k=1}^N \mathbf{A}^{(k)T} \mathbf{B}^{(k)}. \end{aligned} \quad (34)$$

APPENDIX B

PROOF OF MATRIX CALCULUS IDENTITY

We here prove the identity in (23). Let $\mathbf{Y} = \mathbf{X} \circledast \mathbf{W}$ and a colon ($:$) denote the inner product operator. Then,

$$\begin{aligned} q &= \text{Tr} \left(\mathbf{Y} \mathbf{Z} \mathbf{Y}^T \right) \\ &= \text{Tr} \left(\mathbf{Y}^T \mathbf{Y} \mathbf{Z} \right) \\ &= \mathbf{Z} : \mathbf{Y}^T \mathbf{Y}. \end{aligned} \quad (35)$$

We can now obtain the differential

$$\begin{aligned} dq &= \mathbf{Z} : d(\mathbf{Y}^T \mathbf{Y}) \\ &= \mathbf{Z} : \left(\mathbf{Y}^T d\mathbf{Y} + d\mathbf{Y}^T \mathbf{Y} \right) \\ &= \mathbf{Z} : \mathbf{Y}^T d\mathbf{Y} + \mathbf{Z} : d\mathbf{Y}^T \mathbf{Y} \\ &= \mathbf{Z} : \mathbf{Y}^T d\mathbf{Y} + \mathbf{Z}^T : \mathbf{Y}^T d\mathbf{Y} \\ &= \left(\mathbf{Z} + \mathbf{Z}^T \right) : \mathbf{Y}^T d\mathbf{Y} \\ &= \mathbf{Y} \left(\mathbf{Z} + \mathbf{Z}^T \right) : d\mathbf{Y} \\ &= \mathbf{Y} \left(\mathbf{Z} + \mathbf{Z}^T \right) : \mathbf{W} \circledast d\mathbf{X} \\ &= \left(\mathbf{Y} \left(\mathbf{Z} + \mathbf{Z}^T \right) \right) \circledast \mathbf{W} : d\mathbf{X}. \end{aligned} \quad (36)$$

Finally, this implies that

$$\frac{\partial q}{\partial \mathbf{X}} = \left((\mathbf{X} \circledast \mathbf{W}) (\mathbf{Z} + \mathbf{Z}^T) \right) \circledast \mathbf{W}. \quad (37)$$

ACKNOWLEDGMENTS

The authors would like to thank Giuseppe Calvi and Bruno Scalzo Dees for helpful discussions. A.H. is supported by an Imperial College London Presidents Scholarship. K.K. is supported by an EPSRC International Doctoral Scholarship.

REFERENCES

- [1] I. V. Oseledets, “Tensor-train decomposition,” *SIAM Journal on Scientific Computing*, vol. 33, no. 5, pp. 2295–2317, 2011.
- [2] W. Hackbusch and S. Kühn, “A new scheme for the tensor representation,” *Journal of Fourier analysis and applications*, vol. 15, no. 5, pp. 706–722, 2009.
- [3] A. Graves, A.-r. Mohamed, and G. Hinton, “Speech recognition with deep recurrent neural networks,” in *2013 IEEE international conference on acoustics, speech and signal processing*. IEEE, 2013, pp. 6645–6649.
- [4] D. P. Mandic and J. Chambers, *Recurrent neural networks for prediction: learning algorithms, architectures and stability*. John Wiley & Sons, Inc., 2001.
- [5] A. Krizhevsky, I. Sutskever, and G. E. Hinton, “Imagenet classification with deep convolutional neural networks,” in *Advances in neural information processing systems*, 2012, pp. 1097–1105.
- [6] N. Cohen, O. Sharir, and A. Shashua, “On the expressive power of deep learning: A tensor analysis,” in *Conference on Learning Theory*, 2016, pp. 698–728.
- [7] V. Khrulkov, A. Novikov, and I. Oseledets, “Expressive power of recurrent neural networks,” in *International Conference on Learning Representations*, 2018. [Online]. Available: <https://openreview.net/forum?id=S1WRibb0Z>
- [8] V. Khrulkov, O. Hrinchuk, and I. Oseledets, “Generalized tensor models for recurrent neural networks,” *arXiv preprint arXiv:1901.10801*, 2019.
- [9] G. G. Calvi, A. Moniri, M. Mahfouz, Z. Yu, Q. Zhao, and D. P. Mandic, “Tucker tensor layer in fully connected neural networks,” *arXiv preprint arXiv:1903.06133*, 2019.
- [10] A. Novikov, D. Podoprikin, A. Osokin, and D. P. Vetrov, “Tensorizing neural networks,” in *Advances in neural information processing systems*, 2015, pp. 442–450.
- [11] W. Wang, Y. Sun, B. Eriksson, W. Wang, and V. Aggarwal, “Wide compression: Tensor ring nets,” in *Proceedings of the IEEE Conference on Computer Vision and Pattern Recognition*, 2018, pp. 9329–9338.
- [12] E. Stoudenmire and D. J. Schwab, “Supervised learning with tensor networks,” pp. 4799–4807, 2016. [Online]. Available: <http://papers.nips.cc/paper/6211-supervised-learning-with-tensor-networks.pdf>
- [13] A. Novikov, M. Trofimov, and I. Oseledets, “Exponential machines,” *Bulletin of the Polish Academy of Sciences. Technical Sciences*, vol. 66, no. 6, 2018.
- [14] C. Guo, Z. Jie, W. Lu, and D. Poletti, “Matrix product operators for sequence-to-sequence learning,” *Phys. Rev. E*, vol. 98, p. 042114, Oct 2018. [Online]. Available: <https://link.aps.org/doi/10.1103/PhysRevE.98.042114>
- [15] A. Cichocki, D. Mandic, L. De Lathauwer, G. Zhou, Q. Zhao, C. Caiafa, and H. A. PHAN, “Tensor decompositions for signal processing applications: From two-way to multiway component analysis,” *IEEE Signal Processing Magazine*, vol. 32, no. 2, pp. 145–163, March 2015.
- [16] T. G. Kolda and B. W. Bader, “Tensor decompositions and applications,” *SIAM Review*, vol. 51, no. 3, pp. 455–500, September 2009.
- [17] A. Cichocki, N. Lee, I. Oseledets, A.-H. Phan, Q. Zhao, and D. Mandic, “Tensor networks for dimensionality reduction and large-scale optimization: Part 1 low-rank tensor decompositions,” *Foundations and Trends in Machine Learning*, vol. 9, pp. 249–429, 01 2016.
- [18] J. D. Carroll and J.-J. Chang, “Analysis of individual differences in multidimensional scaling via an n-way generalization of eckart-young decomposition,” *Psychometrika*, vol. 35, no. 3, pp. 283–319, 1970.
- [19] R. Harshman, “Foundations of the parafac procedure: Models and conditions for an “explanatory” multimodal factor analysis,” 1970.
- [20] M. H. Stone, “Applications of the theory of boolean rings to general topology,” *Transactions of the American Mathematical Society*, vol. 41, no. 3, pp. 375–481, 1937.
- [21] D. Kingma and J. Ba, “Adam: A method for stochastic optimization,” *International Conference on Learning Representations*, 12 2014.
- [22] F. Chollet *et al.*, “Keras,” <https://github.com/fchollet/keras>, 2015.
- [23] D. Liu, S.-J. Ran, P. Wittek, C. Peng, R. B. García, G. Su, and M. Lewenstein, “Machine learning by unitary tensor network of hierarchical tree structure,” *New Journal of Physics*, vol. 21, no. 7, p. 073059, jul 2019. [Online]. Available: <https://doi.org/10.1088>
- [24] A.-H. Phan, A. Cichocki, I. Oseledets, G. G. Calvi, S. Ahmadi-Asl, and D. P. Mandic, “Tensor networks for latent variable analysis: Higher order canonical polyadic decomposition,” *IEEE transactions on neural networks and learning systems*, 2019.
- [25] S. Rendle, “Factorization machines,” in *2010 IEEE International Conference on Data Mining*. IEEE, 2010, pp. 995–1000.
- [26] M. Blondel, M. Ishihata, A. Fujino, and N. Ueda, “Polynomial networks and factorization machines: New insights and efficient training algorithms,” in *International Conference on Machine Learning*, 2016, pp. 850–858.
- [27] R. Livni, S. Shalev-Shwartz, and O. Shamir, “On the computational efficiency of training neural networks,” in *Advances in neural information processing systems*, 2014, pp. 855–863.
- [28] S. Efthymiou, J. Hidary, and S. Leichenauer, “Tensornetwork for machine learning,” *CoRR*, vol. abs/1906.06329, 2019. [Online]. Available: <http://arxiv.org/abs/1906.06329>
- [29] S. Ioffe and C. Szegedy, “Batch normalization: Accelerating deep network training by reducing internal covariate shift,” 2015, pp. 448–456. [Online]. Available: <http://jmlr.org/proceedings/papers/v37/ioffe15.pdf>
- [30] F. M. Harper and J. A. Konstan, “The movielens datasets: History and context,” *ACM Trans. Interact. Intell. Syst.*, vol. 5, no. 4, pp. 19:1–19:19, Dec. 2015. [Online]. Available: <http://doi.acm.org/10.1145/2827872>
- [31] G. Evenbly and G. Vidal, “Tensor network states and geometry,” *Journal of Statistical Physics*, vol. 145, no. 4, pp. 891–918, 2011.
- [32] H. Zhang and F. Ding, “On the kronecker products and their applications,” *J. Appl. Math.*, vol. 2013, p. 8 pages, 2013. [Online]. Available: <https://doi.org/10.1155/2013/296185>